Sandpiles subjected to sinusoidal drive

J. Cheraghalizadeh ®,* M. A. Seifi MirJafarlou, and M. N. Najafi
Department of Physics, University of Mohaghegh Ardabili, P.O. Box 179, Ardabil, Iran

This paper considers a sandpile model subjected to a sinusoidal external drive with the period T. We develop a theoretical model for the Green's function in a large T limit, which predicts that the avalanches are anisotropic and elongated in the oscillation direction. We track the problem numerically and show that the system additionally shows a regime where the avalanches are elongated in the perpendicular direction with respect to the oscillations. We find a crossover between these two regimes. The power spectrum of avalanche size and the grains wasted from the parallel and perpendicular directions are studied. These functions show power-law behavior in terms of the frequency with exponents, which run with T.

I. INTRODUCTION

Sandpile models are prototypical examples of systems that show self-organized criticality (SOC) that is self-sustaining in a critical state without tuning any external parameter. To cover various SOC systems found in nature, plenty of versions of sandpiles have been introduced so far, each of which addresses an essential aspect of the original sandpile model introduced by Bak, Tang, and Weisenfeld (BTW). The question of how the universality class of the sandpile is changed fueled many studies in the field. The Manna version of sandpiles (Manna model, sometimes called the two-state sandpile model) introduced *stochasticity* to the BTW model [1,2], while the Zhang model [3,4] for sandpiles made a continuous-energy model. There were also directed versions of sandpiles that have been greatly investigated over time [5–7]. The sandpile models were also implemented on top of many host systems like the regular d-dimensional hypercubic lattice [6,8,9], honeycomb lattice [10], Bethe lattice [11], random network [12–15], scale-free network [16,17], small-world network [18–23], and so on. Many aspects of this model are known, like the height correlations [24] and its relation to the other statistical models, like the q-state Potts model and Spanning trees [25,26], loop-erased random walks [27], logarithmic conformal field theories [28–30], and Schramm-Loewner evolution [10,31]. For review see [2,32,33].

The real sandpiles were considered in a few studies. In [34], the properties of real sandpiles on a circular disk were analyzed, where the sand grains were added to the pile after the avalanches subsided. In this study, self-similar avalanches with power-law mass distribution functions were observed and a power spectrum of mass was found to behave like f^{-2} (f being the frequency). Jaeger *et al.* [35] arranged an experimental setup for sandpiles consisting of spherical glass beads or rough aluminum-oxide particles, where the effect of vibration was also tested. For the case without vibrations, serious

deviations from the theoretical predictions were found for the avalanche duration and the power spectrum of the system. It is believed that the deviations from the power-law behavior for the power spectrum predicted by BTW are due to the hysteresis angle (the difference between the threshold angle above which avalanches form and the metastable angle). In fact, for each toppling, the metastable angle should be exceeded by this hysteric angle to allow sands to slide downhill, which causes the periodic occurrence of avalanches in the steady state [36]. The generation of vibrations (which were generated by connecting the system to speakers) as an external drive of the sandpile [35] has shown to have a drastic effect on the spectral properties of the system. Importantly, it causes the system to show a self-similar power spectrum, which for the case of study in [35] it is like $f^{-0.8}$, valid for high-enough frequencies and independent of the type of particles. This problem was analytically followed by considering a periodic external drive. This and the following attempts have been made to understand the dynamic response of a granular pile to vibration, by assuming that the effect of the vibration is equivalent to a white noise. The effect of vibrations and their properties have not been thoroughly investigated in the literature and some limited simulations have been done [37–39]. The relaxation of granular systems like the powder was considered in a few papers [35,37–41] in which the volume fraction was investigated in terms of the intensity and the frequency of the vibrations. In [37,39–41] the authors were able to tackle the problem by replacing the effect of the vibration by white noise within a *potential well* model. Besides the logarithmic decay of the slope with time, which was observed experimentally [35] and explained theoretically [39,40], an important question concerning their universal behaviors remains unanswered: That of whether and how the vibrations modify the geometrical and statistical properties of a sandpile. Regarding the limited theoretical knowledge of sandpiles, the modeling of the oscillating external drive helps to shed much light on its lesser-known aspects. Importantly, modeling the in-plane vibrations generates anisotropy in the system, which has not been examined and characterized in previous studies. Up to
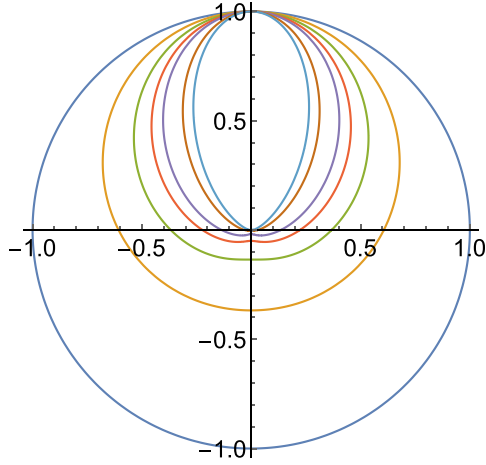
*jafarcheraghalizadeh@gmail.com

FIG. 1. Polar plot for the asymptotic behavior $r \to \infty$ according to Eq. (6). The symmetric circle path is for the isotropic case $\epsilon_0 = 0$ and the most anisotropic one (largest aspect ratio) is for $\epsilon_0 = 1$.

the authors' knowledge, the power spectrum analysis on these systems in terms of external vibration strength was only done in [35]. In this study, we try to fill this gap.

We model the vibrating (periodic external drive) sandpiles with a constant rate of grain addition. To this end, we consider a pile subjected to periodic forcing with a period T. In the local toppling rule, the sands spread in the direction parallel to the vibrations and the perpendicular direction is different. The problem studied here is important from two points of view.

(1) Mathematical point of view. The problem which is studied here is in a sense *the inverse* of the diffusive sandpiles, studied in [42]. More precisely, here we are tracking the sandpiles in which vibrations prevent the avalanches to settle perfectly. Also, in the steady state of the normal sandpile models the recurrent configurations (RC), also referred to as steady state configurations, are statistically constant, while the RCs are replaced by oscillatory RCs, the average of which is a constant. Such vibrating RC states have not been investigated and characterized before.

(2) The second point of view is the experimental perspective. As we stated above, there were some experiments where the sandpile was exposed to vibrations. What the vibrations do is expose an extra force, which can be realized experimentally by preparing a real sandpile on top of a vibrating table. While a more complicated model should be designed for such real situations (like the under-threshold topplings), the first step towards understanding is considering an ideal model which is
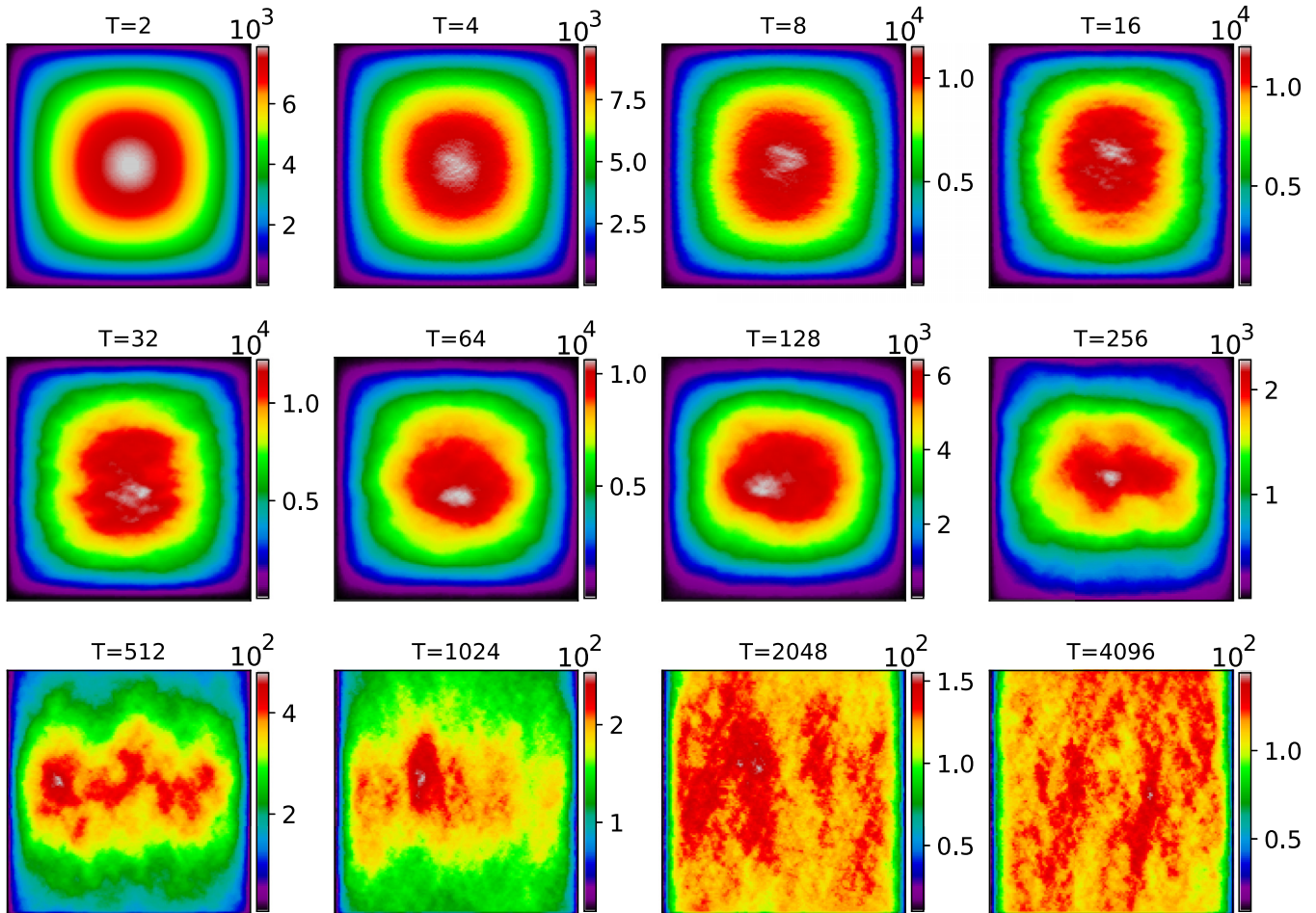

FIG. 2. Total system activity (sum of activity from $t = t_{\text{reached recurrent}}$ till $t = t_{\text{finished}}$, i.e., the time at which the simulation ends) for various T on $L = 256$ lattice. The direction of oscillations (parallel direction) is up-down and the perpendicular direction is left-right.
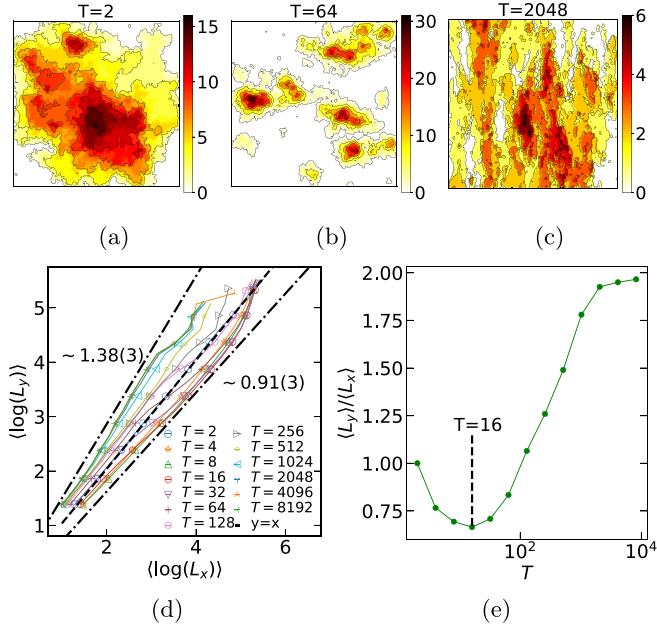
FIG. 3. Finite activity (a) $T = 2$ and $t \in [t_{\text{recurrent}}, t_{\text{recurrent}} + 1000]$ time step (b) $T = 64$ and $t \in [t_{\text{recurrent}}, t_{\text{recurrent}} + 1000]$ time step (c) $T = 2048$ and $t \in [t_{\text{recurrent}}, t_{\text{recurrent}} + 10000]$ time step. For all cases $L = 256$. (d) $\langle \ln L_y \rangle$ in terms of $\langle \ln L_x \rangle$. L_x and L_y show a box size that covers a growing avalanche. (e) $\frac{\langle L_y \rangle}{\langle L_x \rangle}$ in terms of T. Snapshot time delay is $dt = 100$.

easier to handle and gives the main ingredients of the system which we are doing here.

As an observation, we assert and numerically confirm that for the large (small) T values, the avalanches are extended along the direction (perpendicular direction) to the vibrations. We find that the system undergoes a crossover between these two regimes. We report on the associated exponents that monitor the crossover. The power spectrum behaves in a power-law form for all T values, with the exponent which runs with T.

The paper is organized as follows. We introduce the model in the next section. Section III is devoted to the results of the simulations. We close the paper with a conclusion.

II. MODEL

We define a sandpile model under oscillations (oscillatory sandpile model, OSM) on a $L \times L$ lattice and attribute the height variable $\{h_{i,j}\}_{i,j=1}^{L}$ to each site, which takes the values from the range $h_{i,j} \in [1, h_{\text{th}} \equiv 4n]$ (n being an integer number, which is 10 in this paper). When the height of any site (i, j) exceeds the threshold h_{th}, it *topples*, meaning that the site loses h_{th} sand grains, which are distributed over its neighbors. More precisely, when the site (i, j) topples, then $h_{i',j'} \rightarrow h_{i',j'} + \Delta_{i,j;i',j'}^{t}$, where $\Delta_{i,j;i',j'}^{t}$ is a time-dependent (t) matrix as follows:

$$\Delta_{i,j;i',j'}^{t} = \begin{cases} -4n & \text{if } i = i' \text{ and } j = j', \\ n & \text{if } i = i' \pm 1 \text{ and } j = j', \\ \{n[1 \pm \epsilon_0 \sin(\omega t)]\} & \text{if } i = i' \text{ and } j = j' \pm 1, \\ 0 & \text{other}, \end{cases}$$

(1)

where ϵ_0 is the vibration strength parameter, $\omega = \frac{2\pi}{T}$ is the angular frequency, $[x]$ shows the integer value of x, and T is the time period for the oscillations. Note that the oscillations are imposed only in the j direction. Throughout this paper, we call the direction parallel to the direction of oscillations (j) as the *parallel direction*, while the other direction (perpendicular to the oscillations, i) as the *perpendicular* direction. Obviously, the OSM is anisotropic, i.e., the dynamic in the *parallel* direction is different from the one in the *perpendicular* (i) direction.

Now we define the sandpile dynamic. We start with a uniform random configuration in which all the sites are stable. Then we add n sand grains to a randomly chosen site. This operation, called *grain injection*, takes place every Δt time step that is defined in the following. If it is stable again, then we wait for Δt time steps to choose another random site for adding grains. If it becomes unstable, then it topples according to Eq. (1). For the boundary sites, n or $2n$ sand grains are dissipated depending on the position of the boundary site. As a result, the neighboring sites may become unstable and topple in their turn. Therefore, a chain of topplings is triggered. We define *one-time step* $\delta t = 1$ as the time during which *all* the sites of the lattice are tested once for local toppling, after which $t \rightarrow t + \delta t$. After Δt time steps, another random site is chosen to add an external grain, whether or not the previous chain of activities is over: If the chain is over (there are no further unstable sites at some time), then the time is added one by one during which no activity is done until reaching the next time for injection (reaching Δt steps). Therefore, the *avalanches* are not well defined as in the regular sandpiles (chain of topplings between two stable configurations). However, we have some *toppled* sites in any arbitrary time interval $[t_1, t_2]$ which allows us to define avalanches: It is the set of sites that have toppled at least once in this interval where are *unconnected avalanches*. All the geometrical statistical analyses are upon such avalanches in this paper.

In the limit $T = 2$ the effect of oscillations is zero. When T is large, the sand grains tend to diffuse more in the parallel (j) direction in the short timescales and the *avalanches* are expected to extend in this direction. In the limit $T \rightarrow \infty$, the fate of the sandpile depends on t/T. For small times $t/T \ll 1$, the effect of vibrations is negligible, while their effect is maximal for $\omega t \approx \frac{\pi}{2}$. In the opposite limit, i.e., high ω values, one expects that the avalanche is squeezed in the parallel direction and extends more in the perpendicular direction. This is because the timescale for changing the direction of the preferred parallel direction [i.e., the direction to which the sand grains are more likely to topple according to Eq. (1)] due to the oscillations is much smaller than the timescale of the avalanche to diffuse in this direction and the avalanches do not have enough time to extend in the parallel direction. Therefore, we expect the avalanches to be anisotropic and there is a transition point where the preferred alignment changes from the parallel to the perpendicular direction. The observation of this crossover between two regimes and its characterization is the main goal of the present paper. During this crossover (in terms of T) the avalanches change their behavior from perpendicular-direction-squeezed avalanches to parallel-direction-squeezed avalanches. Additionally, we provide some exponents for the
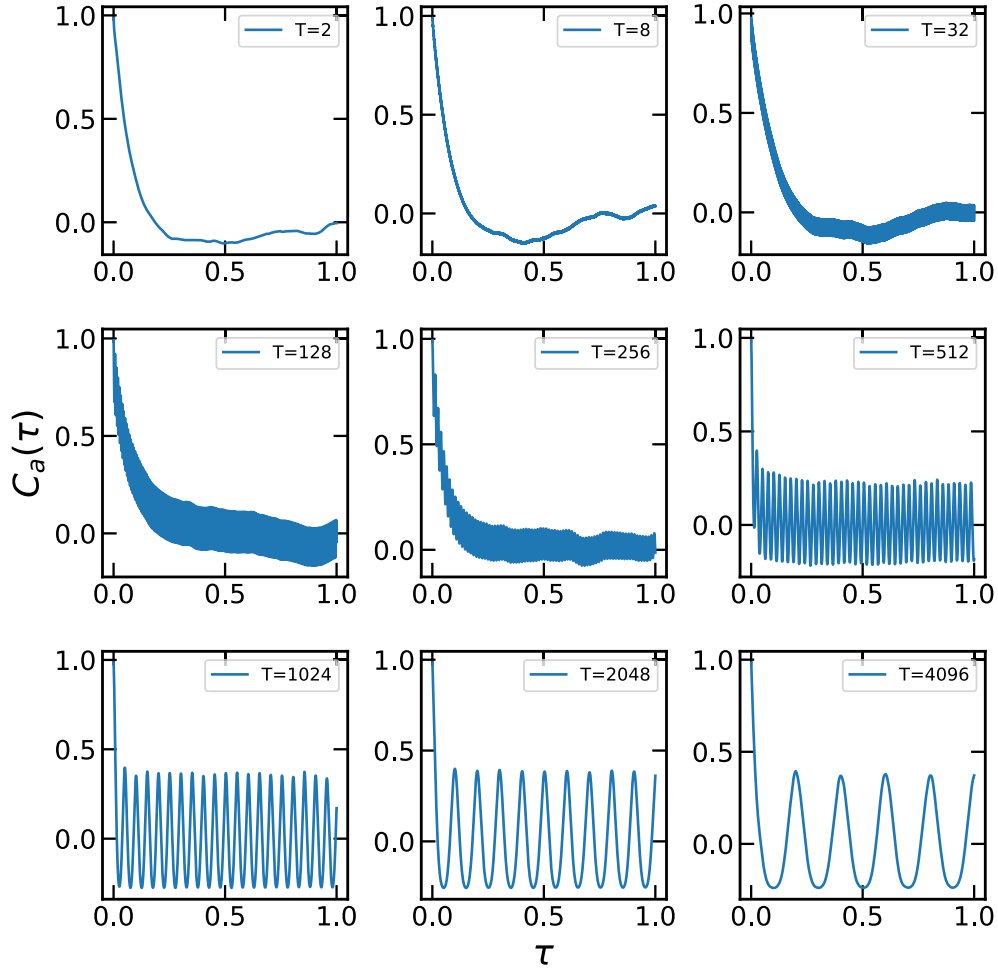
FIG. 4. The system activity ACF for various T on $L = 256$ lattice size. Note that the scale of the x axes is 10^4.

anisotropic elongated avalanches. The power spectral density (PSD, or power spectrum) for the system activity and the dissipated sand grains shows power-law behavior in terms of the frequency some with nontrivial exponents which are different in the sandpile literature.

We consider the following time series. The number of topplings at time t, $a(t)$, which is called activity. The number of grains in the pile at time t, i.e., $m(t)$. These variables do not depend on the sign of bias, i.e., in terms of the Eq. (1) they would be a function of $\sin^2(wt)$ and have the periodicity $\frac{T}{2}$. The number of dissipated grains in the parallel (perpendicular) direction $dn_\parallel(t)$ $[dn_\perp(t)]$ are the other quantities that we investigate here. These variables depend on the sign of the bias field and they have the periodicity T. Note also that $m(t) = m(0) + \frac{t}{\Delta t} - \sum_{t'=1}^{t}[dn_\parallel(t') + dn_\perp(t')]$, i.e., these quantities are not independent. The system's dynamics are divided into two parts. The first stages are called the transient configurations, identified by the height increasing with time and configurations with nonzero probability in the periodic steady state. All of our analyses are done in the latter configurations.

We start our arguments by defining the Green's function $G(t, \mathbf{X}, \mathbf{Y})$ as the probability that the site $\mathbf{X}$ topples in an avalanche at time t created by addition sand grain to the site $\mathbf{Y}$ at $t = 0$. The Green's function satisfies the master

equation ($\mathbf{X} \neq \mathbf{Y}$),

$$G(t + 1, \mathbf{X}, \mathbf{Y}) = \tfrac{1}{4}\{G(t, \mathbf{X} + \mathbf{e}_x, \mathbf{Y}) + G(t, \mathbf{X} - \mathbf{e}_x, \mathbf{Y})$$
$$+ [1 - \epsilon_0 \sin(\omega t)]G(t, \mathbf{X} + \mathbf{e}_y, \mathbf{Y})$$
$$+ [1 + \epsilon_0 \sin(\omega t)]G(t, \mathbf{X} - \mathbf{e}_y, \mathbf{Y})\}. \quad (2)$$

In the continuum limit one obtains ($\mathbf{X} \neq \mathbf{Y}$)

$$\partial_t G(t, \mathbf{X}, \mathbf{Y}) = D_2 \nabla^2 G(t, \mathbf{X}, \mathbf{Y}) - D_1 \epsilon_0 \sin \omega t \, \partial_y G(t, \mathbf{X}, \mathbf{Y}), \quad (3)$$

where $D_1 = \frac{a}{2\delta t}$ and $D_2 = \frac{a^2}{4\delta t}$ are the diffusion coefficients in the scaling limit, a is the lattice constant, and δt is the time difference. Note that the case $\epsilon_0 = 0$ reduces to a simple diffusion equation. The solution to the above equation is complex to find. Instead, let us consider simple cases. The OSM with $\epsilon_0 = 1$ is mapped to a superposition of two *deepest descent sandpile model (DDSM)* with preferred directions $\{nn\}_1 = \{\mathbf{e}_x, \mathbf{e}_y\}$ and $\{nn\}_2 = \{\mathbf{e}'_x, \mathbf{e}_y\}$ [where $\{nn\}$ shows the list of nearest neighbors, $\mathbf{e}_x \equiv (1, 0)$, $\mathbf{e}_y \equiv (0, -1)$, and $\mathbf{e}'_x \equiv (-1, 0)$] just at the moments $\omega t_n = (2n + 1)\frac{\pi}{2}$ (n being an integer number). By the superposition, we mean that the toppling role is a mix of these two models, where, for example, one sand grain goes left, one goes right, and two sand grains go up. The DDSM model was investigated analytically in [43]. For the other times, OSM is equivalent to a variant
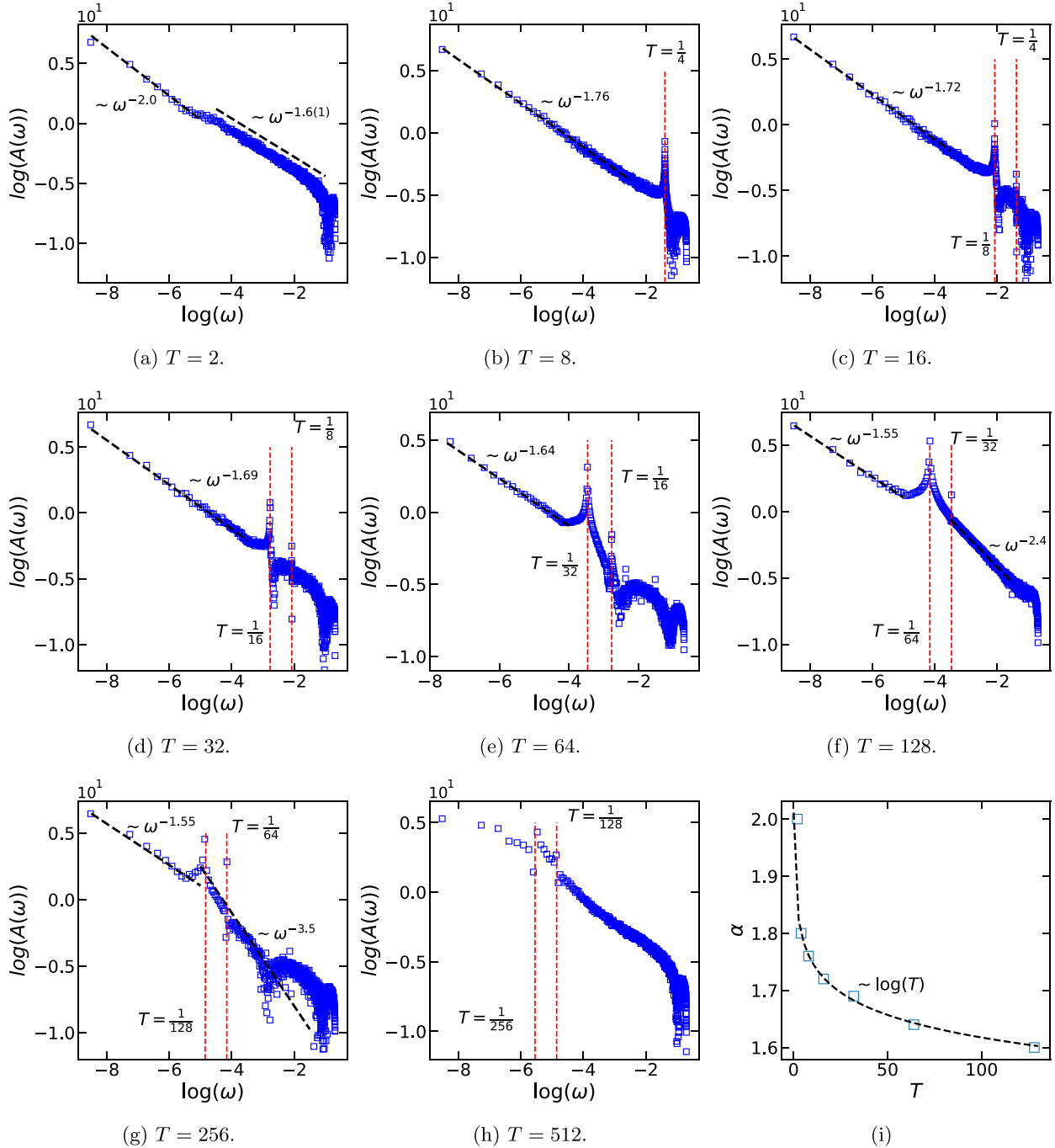
FIG. 5. The system activity PSD for various T at $L = 256$ lattice size. (i) $\alpha_{PS}^{(1)}$ exponents in terms of T for the PSD of the activity time series [i.e., $A(\omega) \sim f^{-\alpha}$]. The fit is the logarithm of T.

of this model where the diffusion in one preferred direction is stronger than in the other direction. Although a complete mapping is restricted to the times t_n, some general features of OSM can be potentially understood in terms of DDSM (easily mapped to a voter model), at least intuitively. Evidently, our model is more complicated since it is directed just in one direction, in contrast to the voter model, for which there are two preferred directions. In the large T limit, during a long time of dynamics, the sand propagation in one direction (up or down) is much larger than in the opposite direction. In this case, $\sin \omega t$ is close to (positive or negative) unity for a long time,

allowing us to talk about the steady state Green's function, which is independent of time, i.e., $g(\mathbf{X}) \equiv G(t, \mathbf{X}, \mathbf{0})$. In this time interval, the system is mapped effectively as a DDSM, with directed diffusion in the $\mathbf{e}_y$ direction, and (far from the boundaries) Eq. (3) becomes [$\mathbf{X} \equiv (x, y)$, and $\sin \omega t \approx 1$]

$$D_2 \big[\partial_x^2 + (\partial_y - \kappa)^2 - \kappa^2 \big] g(\mathbf{X}) = \delta^2(\mathbf{X}), \quad (4)$$

where $\kappa^{-1} \equiv 2 \frac{D_2}{D_1 \epsilon_0} = a/\epsilon_0$ is proportional to the lattice constant. For the case $\mathbf{X} \neq \mathbf{0}$, the solution is

$$g(\mathbf{X}) = e^{\kappa y} [c_1 I_0(\kappa r) + c_2 K_0(\kappa r)], \quad (5)$$
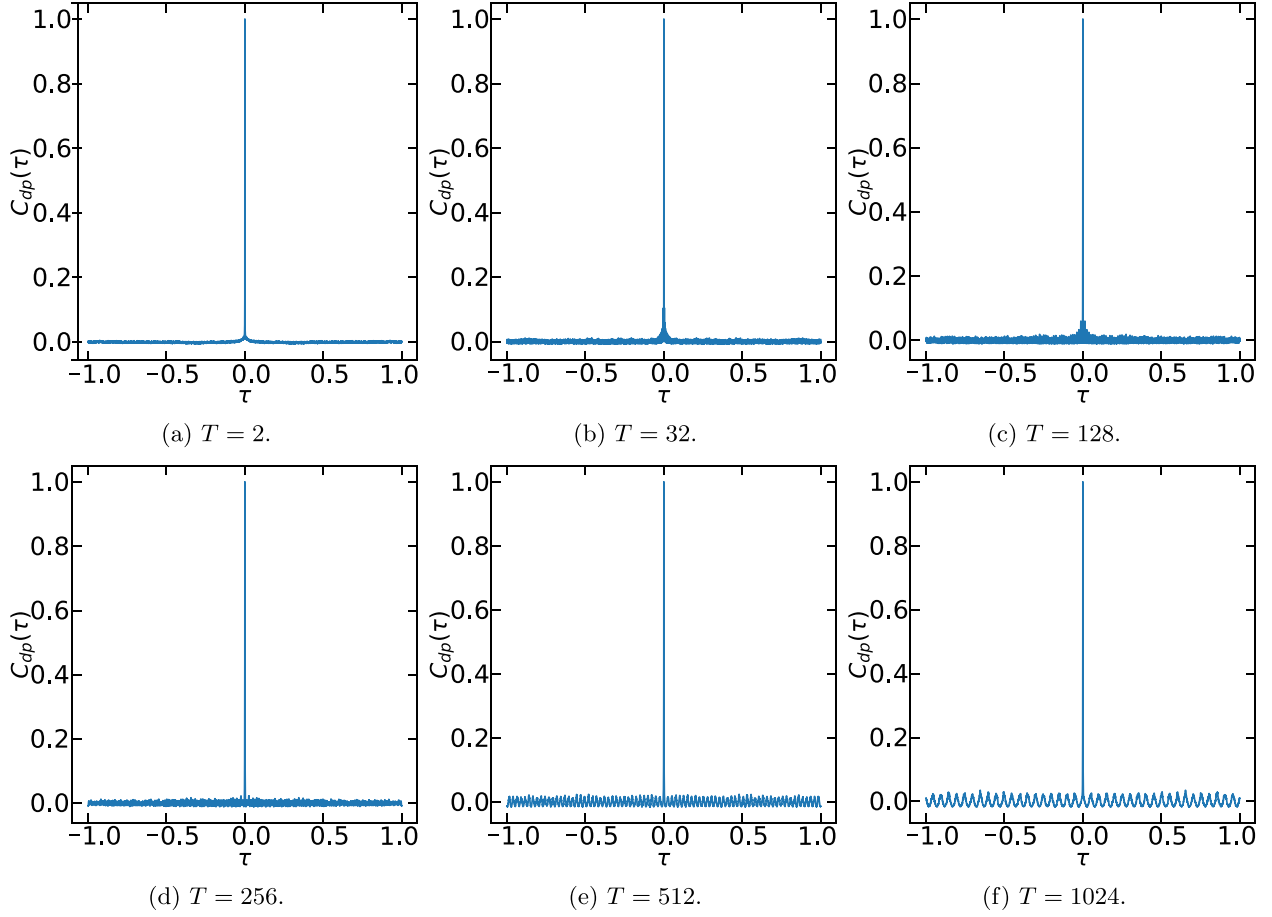
FIG. 6. ACF of sand dissipation in the parallel direction for various T at $L = 256$ lattice size. Note: The scale of the x axes is 10^4.

where $r \equiv \sqrt{x^2 + y^2}$, $I_n(z)$ and $K_n(z)$ are the modified Bessel function of the first and second kinds and c_1 and c_2 are constants to be determined. Since this solution is valid during times shorter or in order to obtain $T/2$, one should not be concerned about exponential growth in the positive y direction. Noting that, in the large r limit, $I_0(\kappa r) \to (1/\sqrt{2\pi\kappa r} \exp[\kappa r])$ and $K_0(\kappa r) \to (\sqrt{\pi/2\kappa r} \exp[-\kappa r])$, one concludes that $c_1 = 0$ and c_2 is nonzero.

Note that, in the absence of oscillations $\epsilon_0 = 0$ or $\kappa = 0$, the system is isotropic and g depends only on r, so that $\frac{1}{r}\frac{d}{dr}[r\frac{d}{dr}g_{\epsilon_0=0}(r)] = \delta(r)$, the solution of which is $\ln r$ as a well-known fact in two-dimensional (2D) ASM. Asymptotically, far from the boundaries, the Green's function behaves like the following [$\mathbf{X} \equiv (r, \theta)$, where $\theta = \tan^{-1}(\frac{y}{x})$]

$$g(r, \theta) \to \begin{cases} e^{\kappa r \cos\theta}\left[\text{const.} - \ln\frac{\kappa r}{2}\right] & \kappa r \ll 1, \\ \frac{1}{\sqrt{\kappa r}}\exp\left[-\kappa r(1 - \cos\theta)\right] & \kappa r \gg 1. \end{cases} \quad (6)$$

The plots for the lower branch are shown in Fig. 1 for a constant r. Increasing ϵ_0 from zero (isotropic case) makes the Green's function more oriented along the y axis as expected. We see that the upper branch in Eq. (6) gives the known logarithmic result for $\epsilon_0 = 0$ ($\kappa = 0$), i.e., the isotropic case. A useful representation of Eq. (5) is as follows ($c_1 = 0$):

$$g(r, \theta) \propto \int_r^\infty \frac{e^{-\kappa(R - r\cos\theta)}}{\sqrt{R^2 - r^2}}dR. \quad (7)$$

To interpret this equation, we take the strategy of the authors of [44]. Let us define $p(R, \theta)$ as the probability that the linear extent of an avalanche is R in the θ direction and $\rho_R(r, \theta)$ as the density of sites [at (r, θ)], covered by the avalanche with the extension R. Then it is easy to see that

$$g(r, \theta) \propto \int_r^\infty p(R, \theta)\rho_R(r, \theta)dR. \quad (8)$$

It was previously shown that for the isotropic case $p^{\epsilon_0=0}(R) \propto R^{-\tau_R}$ ($\tau_R = \frac{1}{4}$) and $\rho_R^{\epsilon_0=0}(r) \propto r^{d_f-2} = r^{-\frac{3}{4}}$, leading to $g_{\epsilon_0=0}(r) \propto \ln r$, see [44,45] for details. In our case, to be consistent with Eq. (6), and also with the isotropic $\epsilon_0 = 0$ case, we propose that ($x \equiv \frac{R}{r}$)

$$p(R, \theta) \propto \frac{e^{-\kappa R(1-\cos\theta)}}{R^{\tau_R}}, \quad \rho_R(r, \theta) \propto r^{d_f-2}\frac{e^{-\kappa r(x-1)\cos\theta}}{\sqrt{x^{\frac{3}{2}} - x^{-\frac{1}{2}}}}, \quad (9)$$

which results in Eq. (7). Note that $P(R)$ has the same angular structure as the lower branch of Eq. (6), see Fig. 1. These analytical arguments predict the directional deformation of the avalanches in the same form as the Green's function.

Now we consider the system with a periodic external drive. For this case, the above equation is expected for long T values and also times that the external drive is only in one direction, while for generic t and T, the behavior is much different. In fact, the system's response to the external drive is determined by comparing t and T, and therefore, we need
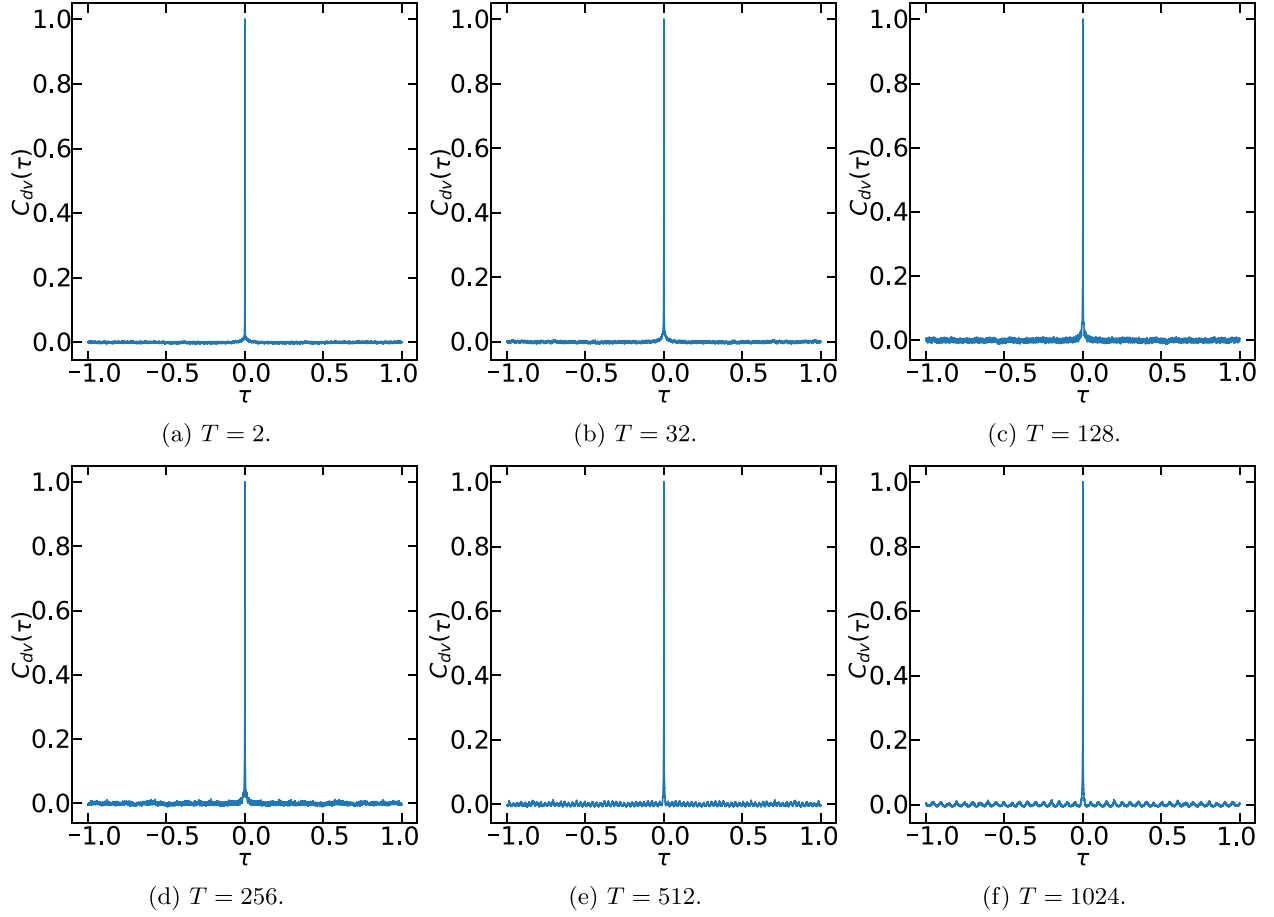
FIG. 7. ACF of sand dissipation in the perpendicular direction of oscillation for various T at $L = 256$ lattice size. Note that the scale of the x axes is 10^4.

dynamic scaling arguments. Generally, the probability that in the SOC state the avalanche has a duration T_d greater than a time t varies as $p(T_d > t) \propto t^{-\tau_d+1}$ in the thermodynamic limit and for large-enough t values, where τ_d is the critical exponent of the avalanche duration, which is $3/2$ for DDSM [43]. As a well-known fact for the finite size systems, the probability distribution function (PDF) of the avalanche duration shows scaling behavior in terms of the size of the system L, so that $\bar{T}_d \equiv \langle T_d \rangle$ shows power-law behavior in terms of L [4,6,46,47]. The same arguments are expected here for our directed sandpile model, although the change of this scaling relation does not hurt our main logic in the following arguments, for which the existence of such a L-dependent timescale is enough. Therefore, we base our arguments in the following on the existence of such a finite timescale. To add the effect of changing the direction of the preferred orientation due to the oscillations, we approximate the sinusoidal function by a periodic step function $f(t) = +\epsilon_0 \, (= -\epsilon_0)$ for $0 \leqslant t < T/2 \, (-T/2 \leqslant t < 0)$ with a period T. As a consequence, the probability that an avalanche experiences a significant change of the preferred direction $p(T_d > T)$ is proportional to $T^{-\frac{1}{2}}$. One then expects two distinct regimes: $T \ll \bar{T}_d$ and $T \gg \bar{T}_d$. For the first case, it is easy to show that $p(T_d > T)$ is considerably large in the thermodynamic limit, while for thesecond case, it is negligibly small. Therefore, for the first case, the avalanches are squeezed in the parallel direction and

are more extended in the perpendicular direction since they do not have enough time to settle or be completely established in the parallel direction. For the second case, the avalanches would not experience this significant change and are more extended in the parallel direction.

We consider the autocorrelation function (ACF) and the power spectral density (PSD) [48] for these time series associated with the quantities introduced above. Given the measurements $\{t_i, x_i\}_{i=1}^N$ where t_i are times, the ACF is defined as

$$C_x(\tau) = \frac{\sum_{i=1}^N \{[x(t_i) - \bar{x}][x(t_i + \tau) - \bar{x}]\}}{\sum_{i=1}^N [x(t_i) - \bar{x}]^2}, \qquad (10)$$

where $x \in \{a, m, dv, dp\}$, $\bar{x}$ shows average of time series, and τ is some time lag. The PSD is the Fourier transform of ACF (the increment of τ is one, i.e., $\Delta \tau = 1$), i.e.,

$$A_x(f) \equiv \sum_{i=1}^N C_x(\tau_i) e^{-i2\pi f \tau_i}, \qquad (11)$$

where f is the frequency.

III. RESULTS AND ANALYSIS

In this section, we present the results of simulating OSM. Throughout this section we set $\epsilon_0 = 1.0$, $n = 10$, and $\Delta t =$
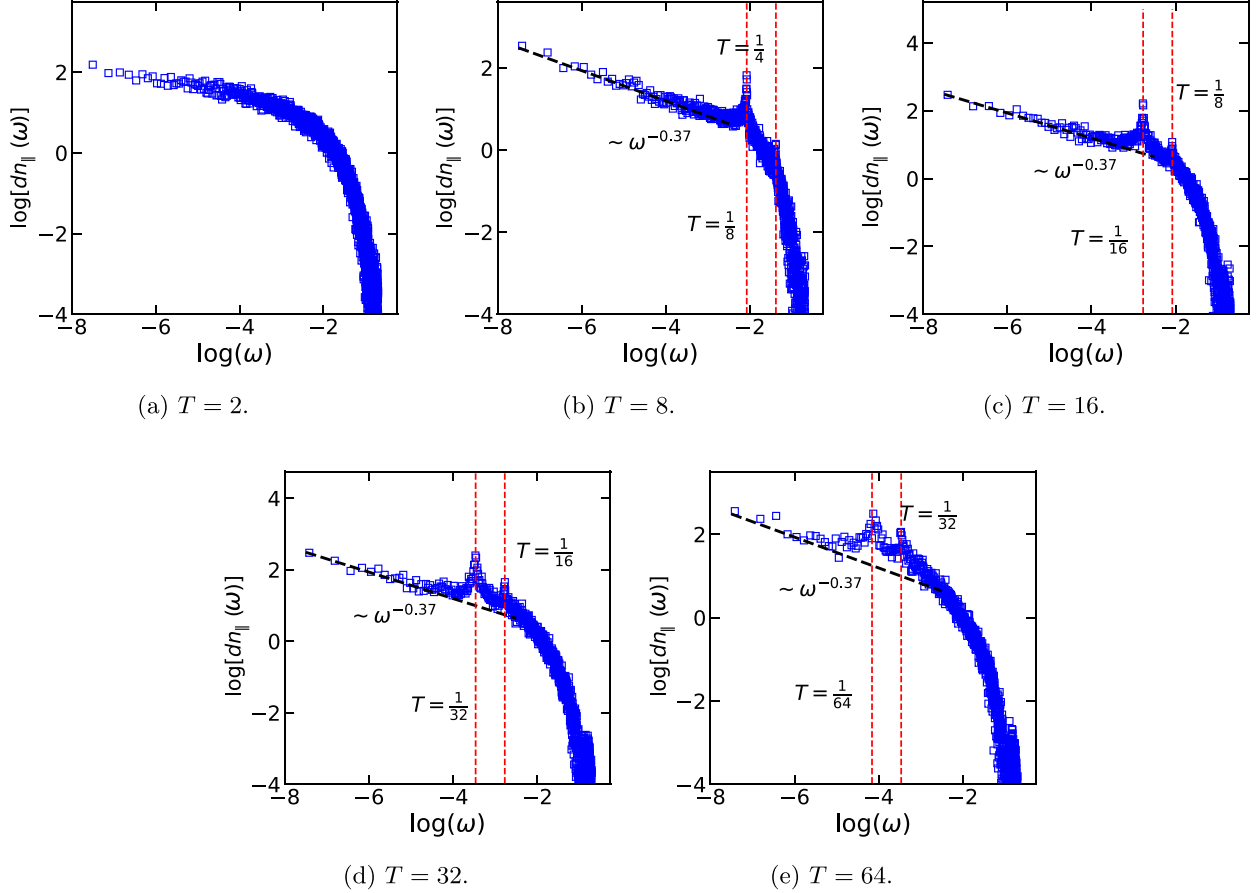
(a) $T = 2$.

(b) $T = 8$.

(c) $T = 16$.

(d) $T = 32$.

(e) $T = 64$.

FIG. 8. PSD for sand dissipation in the parallel direction for various T at $L = 256$ lattice size.

100. Figure 2 shows the total (accumulated) activity of the system is shown in terms of T [note that the case $T = 2$ is isotropic as expected from Eq. (1)]. This helps to figure out how the arguments presented in the previous section work, i.e., for small T values, the avalanches are spatially extended in the perpendicular direction. In contrast, for large T values, their extension in the parallel direction is more than the other direction. Figure 3 shows the same effect for the avalanches.

To quantify this, we define the avalanches as the chain of activities in the interval $t \in [t_{\text{recurrent}}, t_{\text{recurrent}} + 1000]$ and extract the contour lines of the resulting avalanches, see Figs. 3(a), 3(b), and 3(c) ($T = 2, 64$, and 2048, respectively). We calculate the fractal dimension of the resulting avalanches by confining the avalanches in a minimal rectangle with size $L_x \times L_y$ [$L_x = x_{\text{max}} - x_{\text{min}}$, and $L_y = y_{\text{max}} - y_{\text{min}}$, where x_{max} and y_{max} (x_{min} and y_{min}) are maximum (minimum) values for x and y, respectively, for the points on the external frontier of avalanches]. For isotropic avalanches one expects that $\langle \ln L_y \rangle = D_f \langle \ln L_x \rangle$, where $D_f = 1$. We plot $\langle \ln L_y \rangle$ in terms of $\langle \ln L_x \rangle$ in Figs. 3(d) and 3(e). We see that there are two slopes in the figure, and the graphs crossover between them. For a better understanding, let us first consider $T = 2$ (the isotropic case), for which $D_f \approx 1$ is expected. Figure 3(e) shows that the ratio of averages $\frac{\langle L_y \rangle}{\langle L_x \rangle}$ decrease with T for small T values (up to $T^* \approx 16$), and then increases. It is worth mentioning that we should retrieve the ordinary isotropic BTW model as $T \to \infty$. To see this behavior $T \gg T_d$, which is not reached in this figure (due to the simulation time, it was not possible for us to go to this limit). Note also that in the limit $T \to 2$, the ratio goes to 1. The same phenomenon is seen in Fig. 3(d), where the lowest slope is observed in $T = 16$, while the highest value considered is T, for which the slope is approximately 1.38(3). The expected orientational transition is evidenced by changing from $D_f < 1$ to $D_f > 1$. For intermediate T values, the graphs crossover from the first to the second regime, as is seen in the figure. We repeat this calculation for the system sizes $L = 32, 64, 128$, and 256 to control the finite size effects. The associated exponents are more or less the same for all system sizes, which are not shown here. As a response to a sinusoidal external drive, the system's activity is expected to show periodic behavior. Since the activity field is not sensitive to the sign of the external drive, one expects that the activity ACF has a half period of the one for the external drive. Figure 4 shows this function for various rates of period. First, observe that the system without oscillations ($T = 2$) is correlated. As T increases, some tiny oscillations are born the period of which increases by increasing T. For example, for $T = 4096$, the period of ACF is $\tau_0 = 2048 = T/2$. To visualize the structure of the oscillations and the characteristic periods more explicitly, one should study the power spectrum of the time series. PSDs are shown
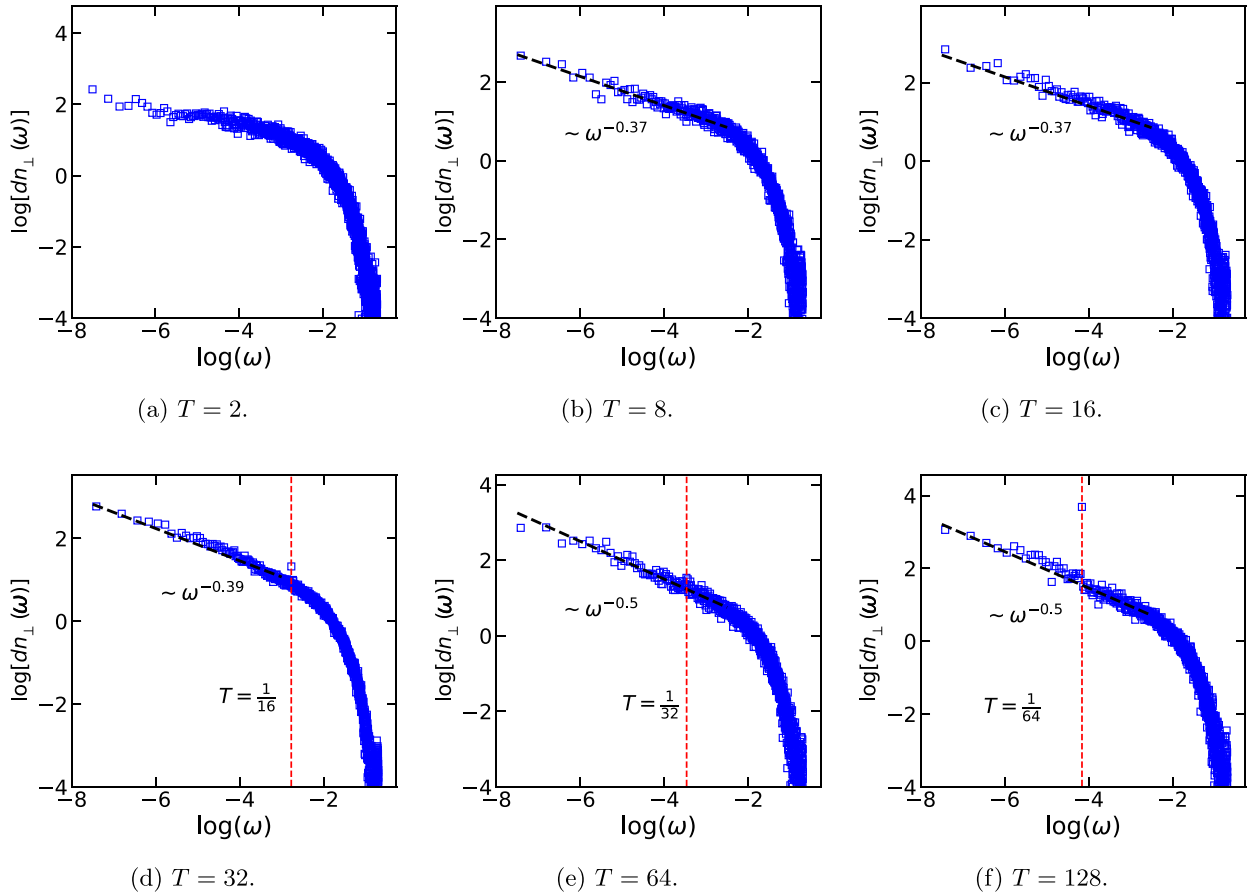
(a) $T = 2$.

(b) $T = 8$.

(c) $T = 16$.

(d) $T = 32$.

(e) $T = 64$.

(f) $T = 128$.

FIG. 9. PSD for sand dissipation in the perpendicular direction for various T at $L = 256$ lattice size.

in Fig. 5, where a multifractal structure (self-similar) structure is observed, reflected in $A(\omega) \propto \omega^{\alpha_{PS}}$, where α_{PS} depends on

FIG. 10. Total system activity (sum of activities from $t_{reached\ recurrent}$ till $t_{finished}$, i.e., The time at which the simulation ends) at $T = 2048$ on $L = 256$ lattice size.

the scale. Observe how the nonoscillating system ($T = 2$) exhibits two regimes: One with the exponent $\alpha_{PS} \simeq 2$ and another with $\alpha_{PS} \simeq 1.6$. It is already known that avalanches in sandpiles are multifractals, but since ACFs (for the BTW model) exponentially decay with time $\alpha_{PS} = 2$ (red noise) is expected for them, as numerically is confirmed. Additionally, PSD functions show peaked structures having their roots in the fact that there are driven oscillations in the ACFs, as we just saw. Indeed, for $\omega \gg \frac{2\pi}{T}$ it has information about single avalanches, while for $\omega \ll \frac{2\pi}{T}$ it tells about the long-time correlations of activity. The regimes are identified with respect to two pronounced peaks which are identified in the figures, one of which is at $f^{-1} = T/2$ and the other one is $f^{-1} = T/4$. One can study the long-time correlations more effectively by subtracting the power spectrum at frequencies $\omega \gg \frac{2\pi}{T}$. The power spectrum exponent in the small frequency regime ($\alpha_{PS}^{(1)}$) decreases by increasing T. This is shown in Fig. 5(i), where a logarithmic decay $\alpha_{PS}^{(1)} = a - b \ln T$ is observed, where $a = 1.88 \pm 0.04$ and $b = 0.06 \pm 0.01$. This fitting is not valid for all ranges of T, i.e., the best fitting is for the range $T \lesssim 128$, where for a self-similar monofractal time series with a Hurst exponent H, the power spectrum is expected to behave like ω^{-2H+1} [49,50], which corresponds in OSM to the Hurst exponent $H = \frac{1}{2}(1 + a - b \ln T)$. While avalanches in OSM are multifractal, a more comprehensive multifractal analysis is necessary to determine the spectrum of the Hurst exponent.
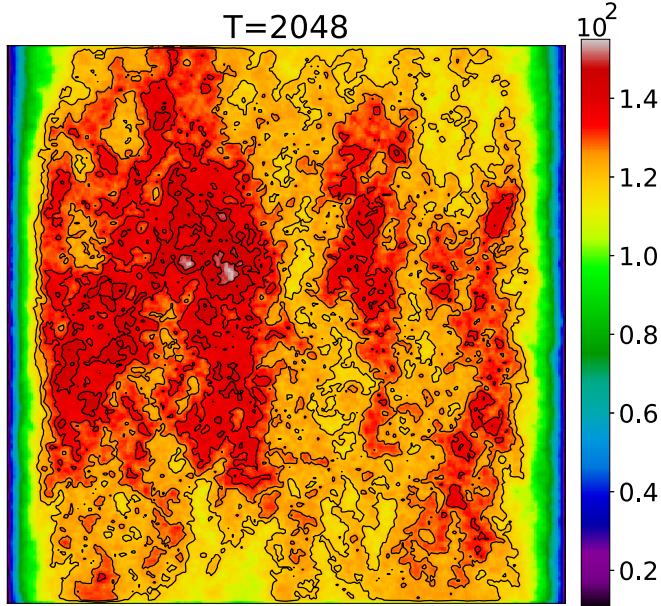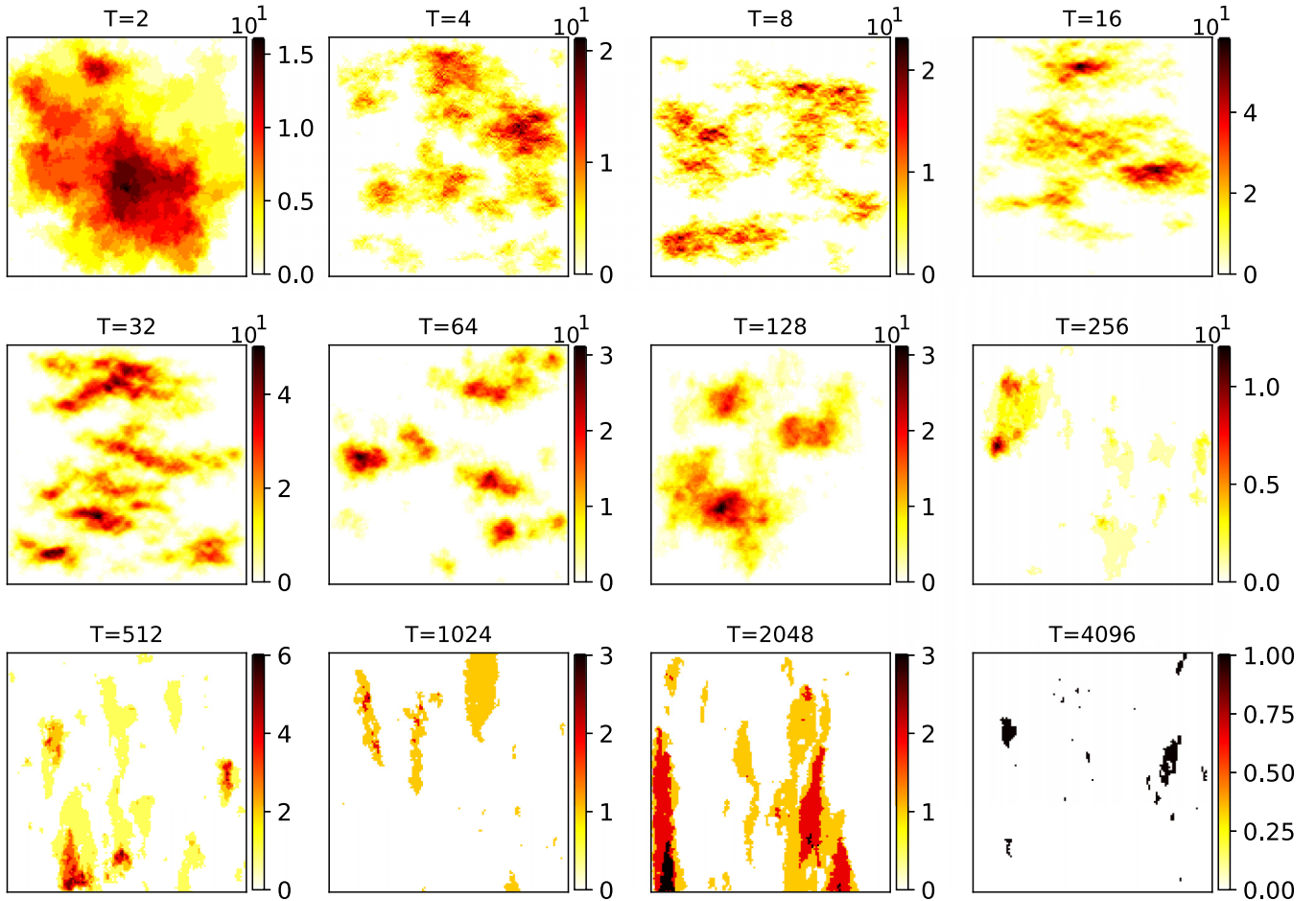
FIG. 11. Finite activity ($t \in [t_{\text{recurrent}}, t_{\text{recurrent}} + 1000]$ time step) in the recurrent regime for various T on $L = 256$ lattice size.

The other independent quantities of interest are the grain dissipation in the parallel ($dn_\parallel$) and perpendicular ($dn_\perp$) directions. The ACF of $dn_\parallel$ and $dn_\perp$ are shown in Figs. 6 and 7 in the Appendix. The decay of ACF for these two quantities is faster than for the activity time series. The corresponding PSD's are shown in Figs. 8 and 9 for $dn_\parallel$ and $dn_\perp$, respectively. It is seen that PSD for $dn_\parallel$ reveals the same spectral structure just like the activity field, while for the PSD of $dn_\perp$ the position of the peaks are not distinguishable. Actually, by looking at the ACF, we observe that the strength of the oscillations is much weaker for $dn_\perp$ than for $dn_\parallel$, which is the reason the peaks in PSD of $dn_\perp$ are not pronounced and distinguishable. PSD functions show power-law decay for both cases for more than two decades (note that the PSD for the nonoscillating SM $T = 2$ can hardly be fitted by a power-law function). The corresponding exponent is fixed (0.37 ± 0.03) for $dn_\parallel$, while a small change is observed with changing T for $dn_\perp$ exponent $\in [0.37 \pm 0.03 - 0.5 \pm 0.03]$.

IV. CONCLUSION

This paper was devoted to the sandpile model subjected to a sinusoidal external drive with the period T. This problem was analyzed analytically and numerically. Using an analytical approach we found that in a large T limit, the Green's function and the avalanches are anisotropic and elongated in the oscillation direction. In particular, we found that in the thermodynamic limit and for the times $\omega t \approx \frac{\pi}{2}$ the Green's function is approximately a multiplication of an exponential term and a modified Bessel function. We considered the problem numerically and showed that, in the intermediate T values, the system is in a regime in which the avalanches are elongated in the perpendicular direction with respect to the oscillations. The transition region between these two regimes is identified by measuring the scaling relation between parallel and perpendicular spatial scales. The power spectrum of avalanche size and the grains wasted from the parallel and perpendicular directions are studied. In agreement with previous studies (like [35]), we find that this simple model generates a flicker ($1/f$) noise, i.e., the power spectrum shows a power-law behavior in terms of the frequency with a T-dependent exponent.

APPENDIX: ACTIVITY FIELD

Figure 2 shows the activity as a function of various T. It shows stretching in the opposite direction of oscillation for

$2 < T < 256$ and for $T > 256$, stretching in the direction of oscillation. Figure 10 shows $T = 2048$ in a large frame with contour lines.

Figure 11 shows the system activity in a finite time step, i.e., $t \in [t_{\text{recurrent}}, t_{\text{recurrent}} + t_{\text{finite}}]$. This figure shows the toppling number in the recurrent regime

for $t = 1000$ time steps. This figure shows system activity decreases for $T \geqslant 256$. Figures 3(a) and 3(b) show finite system activity for $T = 2$ and $T = 64$ with contour lines in large scale, and also Fig. 3(c) shows $T = 2048$ for $t = 10\,000$ time steps in the recurrent regime. It shows the fact that the activity for large T is significantly low.

[1] S. Manna, J. Phys. A: Math. Gen. **24**, L363 (1991).

[2] D. Dhar, Physica A **270**, 69 (1999).

[3] S. Lübeck, Phys. Rev. E **56**, 1590 (1997).

[4] A. Chessa, H. E. Stanley, A. Vespignani, and S. Zapperi, Phys. Rev. E **59**, R12 (1999).

[5] R. Pastor-Satorras and A. Vespignani, J. Phys. A: Math. Gen. **33**, L33 (2000).

[6] D. Dhar, Physica A **263**, 4 (1999).

[7] J. Hasty and K. Wiesenfeld, Phys. Rev. Lett. **81**, 1722 (1998).

[8] A. Ben-Hur and O. Biham, Phys. Rev. E **53**, R1317(R) (1996).

[9] M. Najafi, J. Phys. A: Math. Theor. **49**, 335003 (2016).

[10] M. N. Najafi, S. Moghimi-Araghi, and S. Rouhani, Phys. Rev. E **85**, 051104 (2012).

[11] D. Dhar and S. Majumdar, J. Phys. A: Math. Gen. **23**, 4333 (1990).

[12] M. Najafi, Phys. Lett. A **378**, 2008 (2014).

[13] P. Fronczak, A. Fronczak, and J. A. Hołyst, Phys. Rev. E **73**, 046117 (2006).

[14] E. Bonabeau, J. Phys. Soc. Jpn. **64**, 327 (1995).

[15] F. Redig, W. Ruszel, and E. Saada, J. Stat. Phys. **147**, 653 (2012).

[16] R. Karmakar and S. Manna, J. Phys. A: Math. Gen. **38**, L87 (2005).

[17] D.-S. Lee, K.-I. Goh, B. Kahng, and D. Kim, Physica A **338**, 84 (2004).

[18] H. Bhaumik and S. B. Santra, Phys. Rev. E **88**, 062817 (2013).

[19] G.-J. Pan, D.-M. Zhang, Y.-P. Yin, and M.-H. He, Physica A **383**, 435 (2007).

[20] H. Bhaumik and S. Santra, Physica A **511**, 358 (2018).

[21] M. Hoore and S. Moghimi-Araghi, J. Phys. A: Math. Theor. **46**, 195001 (2013).

[22] M. N. Najafi and H. Dashti-Naserabadi, Phys. Rev. E **97**, 032108 (2018).

[23] J. Lahtinen, J. Kertész, and K. Kaski, Physica A **349**, 535 (2005).

[24] S. N. Majumdar and D. Dhar, J. Phys. A: Math. Gen. **24**, L357 (1991).

[25] S. N. Majumdar and D. Dhar, Physica A **185**, 129 (1992).

[26] S. S. Manna, D. Dhar, and S. N. Majumdar, Phys. Rev. A **46**, R4471(R) (1992).

[27] S. N. Majumdar, Phys. Rev. Lett. **68**, 2329 (1992).

[28] G. Piroux and P. Ruelle, J. Stat. Mech.: Theory Exp. (2004) P10005.

[29] S. Moghimi-Araghi, M. Rajabpour, and S. Rouhani, Nucl. Phys. B **718**, 362 (2005).

[30] P. Ruelle, J. Phys. A: Math. Theor. **46**, 494014 (2013).

[31] A. A. Saberi, S. Moghimi-Araghi, H. Dashti-Naserabadi, and S. Rouhani, Phys. Rev. E **79**, 031121 (2009).

[32] M. Najafi, S. Tizdast, and J. Cheraghalizadeh, Phys. Scr. **96**, 112001 (2021).

[33] D. Marković and C. Gros, Phys. Rep. **536**, 41 (2014).

[34] G. A. Held, D. H. Solina, D. T. Keane, W. J. Haag, P. M. Horn, and G. Grinstein, Phys. Rev. Lett. **65**, 1120 (1990).

[35] H. M. Jaeger, C. H. Liu, and S. R. Nagel, Phys. Rev. Lett. **62**, 40 (1989).

[36] R. A. Bagnold, *The Physics of Blown Sand and Desert Dunes* (Courier Corporation, Mineola, New York, 2012)

[37] A. Mehta and G. C. Barker, Phys. Rev. Lett. **67**, 394 (1991).

[38] G. C. Barker and A. Mehta, Phys. Rev. A **45**, 3435 (1992).

[39] G. C. Barker and A. Mehta, Phys. Rev. E **47**, 184 (1993).

[40] T. Duke, G. Barker, and A. Mehta, Europhys. Lett. **13**, 19 (1990).

[41] A. Mehta and S. Edwards, Physica A **168**, 714 (1990).

[42] M. N. Najafi and Z. Moghadam, Phys. Rev. E **99**, 042120 (2019).

[43] D. Dhar and R. Ramaswamy, Phys. Rev. Lett. **63**, 1659 (1989).

[44] D. V. Ktitarev, S. Lübeck, P. Grassberger, and V. B. Priezzhev, Phys. Rev. E **61**, 81 (2000).

[45] H. Dashti-Naserabadi and M. N. Najafi, Phys. Rev. E **91**, 052145 (2015).

[46] T. Hwa and M. Kardar, Phys. Rev. A **45**, 7002 (1992).

[47] P. Grassberger and S. Manna, Journal de Physique **51**, 1077 (1990).

[48] L. Laurson, M. J. Alava, and S. Zapperi, J. Stat. Mech.: Theory Exp. (2005) L11001.

[49] F. Gharari, K. Arias-Calluari, F. Alonso-Marroquin, and M. N. Najafi, Phys. Rev. E **104**, 054140 (2021).

[50] G. Samorodnitsky, *Stochastic Processes and Long Range Dependence* (Springer, Cham, 2016), Vol. 26.